Hindawi
Complexity
Volume 2020, Article ID 8879045, 10 pages
https://doi.org/10.1155/2020/8879045

Research Article

Adaptive Robust SMC-Based AGC Auxiliary Service Control for ESS-Integrated PV/Wind Station

Xiao-Ling Su,[1,2] **Zheng-Kui Zhao**,[1,2] **Yang Si**,[2] **and Yong-Qing Guo**[2]

[1]*School of Water Resources and Electric Power, Qinghai University, Xining 810016, China*
[2]*Qinghai Key Lab of Efficient Utilization of Clean Energy (Tus-Institute for Renewable Energy), Qinghai University, Xining 810016, China*

Correspondence should be addressed to Xiao-Ling Su; suxiaoling@qhu.edu.cn

Received 19 August 2020; Revised 11 September 2020; Accepted 18 September 2020; Published 7 October 2020

Academic Editor: Qiang Chen

Copyright © 2020 Xiao-Ling Su et al. This is an open access article distributed under the Creative Commons Attribution License, which permits unrestricted use, distribution, and reproduction in any medium, provided the original work is properly cited.

Power source structure has developed significantly because of the increasing share of renewable energy sources (RESs) in the power system. RESs bring inevitable impacts on power system frequency, voltage regulation, and power system stability. The conventional automatic generation control (AGC) loops which relay only on the synchronous generating units cannot meet the requirements of these new circumstances. This paper presents an ESS-integrated PV/wind station topology and its control structure for AGC auxiliary service in order to provide existing RESs the additional functionality of AGC auxiliary service without changing their control strategies conceived for MPPT mode. The shifting operation modes and external disturbances make ESSs in an ESS-integrated PV/wind station inherently nonlinear and time variable. Therefore, an adaptive robust sliding-mode control (ARSMC) system is proposed. The ARSMC colligates the advantages of adaptive control and SMC contains state feedback term, robust control term, and adaptive compensation term. The strictly logical and rigorous proof using Lyapunov stability analysis indicates the ARSMC system is insensitive to parametric uncertainties and external disturbances; meanwhile, it guarantees fast response speed and high control precision. The case studies on NI-PXI platform validate the effectiveness of the proposed approach.

1. Introduction

Power systems see more and more photovoltaic (PV) and wind generation integration. Within increasing renewable energy sources (RESs) penetration level, despite the advantages like environmental friendly and sustainable development, they also bring problems to the utility grid [1–3]. Adjusting power source structure brings an inevitable impact on power system primary frequency response due to the conventional generators reduction and consequent loss of inertia [4]. Therefore the provision of ancillary services is becoming an increasingly challenging task to system operation.

To deal with these issues, some grid corporation released related regulation and technical standards requesting fast frequency response from PV station and wind farm [5]. Xu et al. [6] proposed dynamic gain tuning control approach for AGC with effects of wind power. Wei et al. [7] proposed an optimal automatic generation controllers in a multiarea interconnected power system with utility-scale PV plants. In general, the typical PV and wind generation operate with maximum power point tracking mode [8–10], and the corresponding control algorithms have been developed and refined along the years, being now a mature technology available in the market. It is nearly impractical to request primary frequency response from these intermittent RESs. And the resultant damages of reserve capacity requirements from RESs are solar/wind power curtailment and lower economic efficiency.

Energy storage systems (ESSs) offer a promising capability of voltage and frequency control for power systems due to recent developments in technologies and plummeting cost [11–14]. Research work indicates that one 10 MW/3.66 MWh battery energy storage system can replace a

36 MW conventional automatic generation control (AGC) units without compromising on the AGC performance of the system for day-to-day variations experienced in the system load [15]. Using ESSs to add regulation capacity and improve dynamic performance of AGC, particularly at the high RESs penetration power systems, is a feasible solution [16–18].

Therefore, it is more practical to use commercial PV/wind generation and add extra customized ESSs to provide extra functionalities, namely, ESS-integrated PV/wind stations. The ESSs can eliminate peak and filling the through for PV/wind generation system, equip these stations with fast frequency response, and avoid voltage fluctuations and other power quality issues in the main grid. These features are important as prime movers are renewable energy sources which are characterized by having a stochastic and intermittent behavior.

Beside fast dynamic response, the ESSs are expected to have the characteristics of high control precision and strong antidisturbance capacity, along with the basic requirements like high efficiency and low output current total harmonics distortion. Many techniques have been proposed for ESSs to achieve those control objectives, including proportional-integral-derivative control, model-based control, robust control, and fuzzy control [19–24]. Most likely, traditional control technique only guarantees the desired closed-loop response at the expected operating point, and there are trade-offs between control like performances response speed, static precision, robustness, and tracking performance [25–28]. In addition, power electronic equipment and disturbance give ESSs multivariable structure and highly coupled nonlinearity which brings great challenges to conventional control techniques. Hence, it seems natural to explore other nonlinear controls that can overcome the uncertain challenges and to achieve better compensation and global stability in all operation modes.

Sliding-mode control (SMC) [29–31] is one of the most effective nonlinear robust control strategies since it provides the system dynamics with an invariance property to uncertainties once the system dynamics is controlled in the sliding mode [32, 33]. SMC has been applied to ESSs for frequency regulation [34–36], power management [37], operation state [38], and voltage control [39]. Morstyn et al. [40] proposed a multiagent sliding-mode control for state of charge balancing between battery energy storage systems. The switching frequency variable or chattering is an inherent problem of SMC, and many intelligent control strategies have been used to improve the conventional SMC [41, 42] and avoid chattering. Sebaaly et al. [43] proposed a constant switching frequency operation that allows chattering compensation. Wang et al. [44] proposed SMC-based ESSs to improve the controllability of the microgrid and guarantee seamless transition between its grid connected and islanded operation modes and use PWM to avoid chattering problems. Su et al. [45] developed an adaptive sliding-mode control with hysteresis control strategy for hybrid ESSs to eliminate the current fluctuating and improve its operating stability.

ESSs in practical ESS-integrated PV/wind stations face various disturbances continuously, and these uncertainties and parameter variations make accurate mathematical model building challenging. More seriously, detection limitation and time delay bring more problems to the control system. It is very difficult to achieve outstanding results by conventional SMC. Therefore, this paper proposes an adaptive robust sliding-mode control (ARSMC) system to colligate the advantages of adaptive control and SMC, eliminate the control error under various disturbances, and guarantee fast response to AGC demand, providing qualitative improvements over existing AGC auxiliary service.

2. Proposed ESS-Integrated PV/Wind Station

In this section, the construction of the proposed ESS-integrated PV/wind station is presented in Figure 1, which includes photovoltaic (PV) system, wind generation, and ESSs. The ESS-integrated PV/wind station is connected to the power grid through a circuit breaker (CB) and transformer.

Note that most PV/wind stations integrate to the utility network through cable or overhead line and the RESs output power variations are more likely to cause voltage fluctuations or voltage sags. These problems may enforce RESs disconnection from the power grid. Therefore, it is necessary to use the ESSs to smooth active and reactive power and improve the power quality.

The ESSs can flexibly import/export power from/to the grid and compensate the power variations or reduce the power fluctuations caused by the RESs. It also can fix the station output voltage and frequency or response to power grid dispatching from AGC.

3. AGC Auxiliary Service Control

The control structure of ESS-integrated PV/wind station-based AGC auxiliary service control is shown in Figure 2. All generators in power systems operate based on daily dispatch schedule of dispatching center. Meanwhile, AGC monitor network parameters like frequency, tie-line power flow, and output power of generators calculate the area control error (ACE) according to the control scheme.

Once the voltage/frequency reaches a boundary layer, a voltage/frequency regulation power is produced, and it is defined as follows:

$$\Delta P_{\Sigma}^{\text{request}} = \sum_{i=1,2,3,\cdots} \Delta P_{\Sigma \text{Ci}}^{\text{request}} + \sum_{i=1,2,3,\cdots} \Delta P_{\Sigma \text{Li}}^{\text{request}}, \quad (1)$$

where $\Delta P_{\Sigma}^{\text{request}}$ is the total amount power demand that contains three time scales. They are $\Delta P_{\Sigma}^{\text{daily}\times\text{request}}$, $\Delta P_{\Sigma}^{\text{hourly}\times\text{request}}$, and $\Delta P_{\Sigma}^{\text{minutes}\times\text{request}}$. $\Delta P_{\Sigma C}^{\text{request}}$ is the power demand from conventional power plant (e.g., frequency regulation power plants). $\Delta P_{\Sigma L}^{\text{request}}$ is the power demand from ESS-integrated PV/wind station.

Once the local energy management system (LEMS) of the ESS-integrated PV/wind station receives the dispatch instruction or $\Delta P_{\Sigma L}^{\text{request}}$, it decomposes as

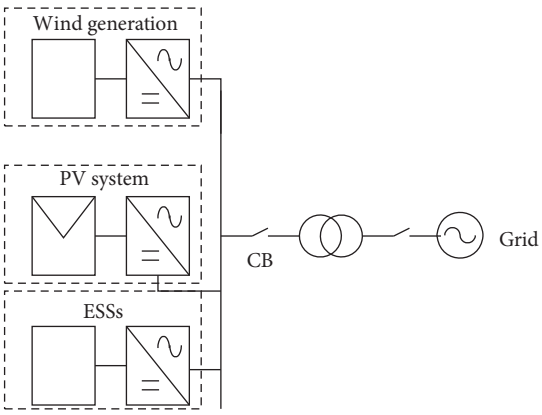

Figure 1: ESS-integrated PV/wind station.

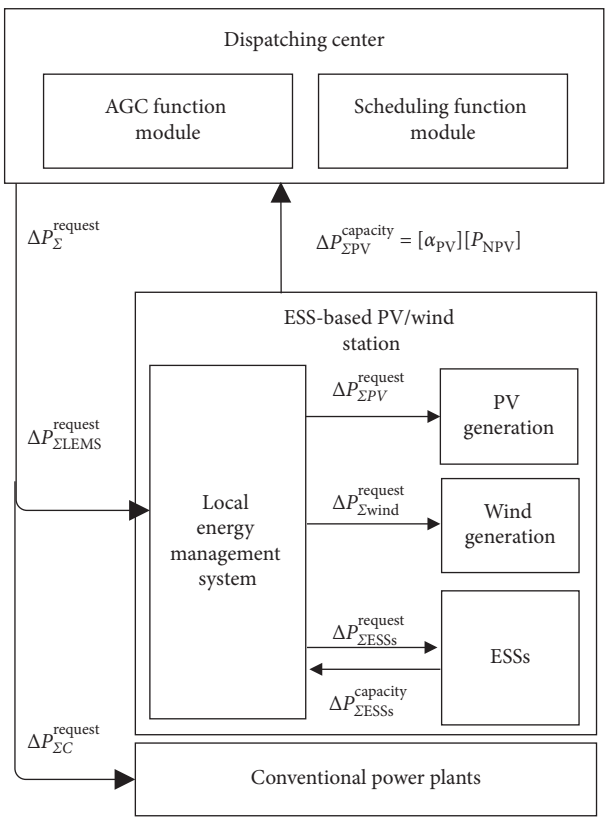

Figure 2: Control structure of ESS-integrated PV/wind station-based AGC auxiliary service.

$$\Delta P_{\Sigma L}^{\text{request}} = \Delta P_{\Sigma PV}^{\text{request}} + \Delta P_{\Sigma wind}^{\text{request}} + \Delta P_{\Sigma ESSs}^{\text{request}}, \tag{2}$$

where $\Delta P_{\Sigma PV}^{\text{request}}$ is the power demand from PV generation. $\Delta P_{\Sigma wind}^{\text{request}}$ is the power demand from wind generation, and $\Delta P_{\Sigma ESSs}^{\text{request}}$ is the power demand from ESSs. There are three operation modes for ESSs:

Mode 1 is the local control mode, which means the ESSs are controlled by LEMS with the shortest communication delay and most flexible and fastest response. ESS-integrated PV/wind station operates as a self-control unit. (a) Charge/discharge based on SOC and the station operation status, for example, storage surplus electricity to reduce solar/wind power curtailment. (b) Smooth RESs output power. ESSs compensate the power variations or reduce the power fluctuations caused by PV/wind generation. (c) Voltage/frequency control. ESSs fix the ESS-integrated PV/wind station output voltage and frequency.

Mode 2 is the frequency/voltage regulation response mode. ESSs generate power according to $\Delta P_{\Sigma ESSs}^{\text{request}}$, quickly responding to the director of AGC.

Mode 3 is the dispatch curve follow mode. ESSs are controlled to follow the dispatch curve or to compensate PV/wind generation to decrease prediction error.

After each control cycle, ESSs feedback their status including the maximum adjustable capacity and time to LEMS. Then LEMS integrates all system parameters as adjustable capacity of ESS-integrated PV/wind station and feedback to dispatching center:

$$\Delta P_{\Sigma L}^{\text{capacity}} = \Delta P_{\Sigma PV}^{\text{capacity}} + \Delta P_{\Sigma wind}^{\text{capacity}} + \Delta P_{\Sigma ESSs}^{\text{capacity}} = \left[\alpha_j\right]\left[P_{Nj}\right], \tag{3}$$

where $[P_j]$ is the rated power of each generation unit. $[\alpha_j]$ is a coefficient matrix, and α_j is the corresponding adjustment coefficient.

The AGC auxiliary service control is integrated with existing AGC control strategies for voltage/frequency regulation and power dispatching. Power grid dispatching center only needs to add an instruction allocation module for the ESS-integrated PV/wind station and update its coefficient matrix $[\alpha_j]$. Achieve the mutual cooperation of frequency regulation resources within fewer changes in the AGC system service modules, which is greatly engineering significant.

4. ESSs Modeling and ARSMC System

In this section, the model of the ESS in PV station and the proposed ARSMC system are presented.

4.1. ESSs Modeling. The optimization objectives of a single ESS can be summarized as follows.

Figure 3 shows the circuit topology of the ESS in ESS-integrated PV/wind station. The ESS consists an electric battery and bidirectional DC-to-AC converter with inductor-capacitor (LC) filter are connected to the AC bus together with the RESs.

In this figure, u_a, u_b, u_c are the AC bus voltages (per phase) and i_a, i_b, i_c are the AC currents (per phase) of the ESSs, and the convertor always works symmetrically. L_a, L_b, L_c and C_{fa}, C_{fb}, C_{fc} are the filter inductor and capacitor values, respectively. r_a, r_b, r_c represent the equivalent series resistor (ESR) of the converter, inductor, and power line. r_{fa}, r_{fb}, r_{fc} represent the ESR of the filter capacitor.

The states of the switches of the n-th leg ($n = 1, 2, 3$) can be represented by the time-dependent variable S_n and

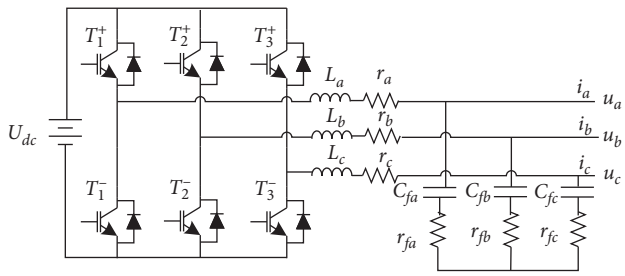

Figure 3: Circuit topology of the ESS in ESS-integrated PV/wind station.

defined as $S_n = 1$, if T_n^+ is on and T_n^- is off, while $S_n = 0$, if T_n^- is on and T_n^+ is off.

This switching strategy, together with a small dead time generator is able to avoid internal shorts between the two switches of each bridge leg, and the switches will be in complementary states. Assuming that compared to the modulation and natural frequencies, the switching frequency is relatively high. Therefore, the equivalent dynamic model of Figure 3 is obtained as shown in Figure 4, where s is the Laplace operator; the power gain is defined as $k_{\mathrm{PWM}} = (U_{\mathrm{dc}}/u_{\mathrm{tri}})$, where u_{tri} is the amplitude of a triangular carrier signal.

Therefore, the dynamic equation of the ESS during the positive-half period can be represented as

$$\begin{cases} L\dfrac{\mathrm{d}i_a}{\mathrm{d}t} = u_a - ri_a + \dfrac{s_b + s_c - 2s_a}{3}U_{\mathrm{dc}}, \\ L\dfrac{\mathrm{d}i_b}{\mathrm{d}t} = u_b - ri_b + \dfrac{s_a + s_c - 2s_b}{3}U_{\mathrm{dc}}, \\ L\dfrac{\mathrm{d}i_c}{\mathrm{d}t} = u_c - ri_c + \dfrac{s_a + s_b - 2s_c}{3}U_{\mathrm{dc}}, \\ C\dfrac{\mathrm{d}U_{\mathrm{dc}}}{\mathrm{d}t} = s_a i_a + s_b i_b + s_c i_c - i_{\mathrm{dc}}. \end{cases} \tag{4}$$

And the dynamic equation of the ESSs under dq0 synchronous rotating coordinate system can be represented as

$$\begin{cases} u_d = L\dfrac{\mathrm{d}i_d}{\mathrm{d}t} - \omega L i_q + ri_d + s_d U_{\mathrm{dc}}, \\ u_q = L\dfrac{\mathrm{d}i_q}{\mathrm{d}t} + \omega L i_d + ri_q + s_q U_{\mathrm{dc}}, \\ \dfrac{\mathrm{d}U_{\mathrm{dc}}}{\mathrm{d}t} = -\dfrac{i_{\mathrm{dc}}}{C} + \dfrac{1}{C}\left(s_d i_d + s_q i_q\right), \end{cases} \tag{5}$$

where u_d, u_q and i_d, i_q are the AC voltage and current under dq0 synchronous rotating coordinate system, respectively. u_{cond} and u_{conq} are the control signal under dq0 synchronous rotating coordinate system. L is the equivalent inductor, and C is the capacitor value on the convertor side. r represents the equivalent series resistor of the converter, inductor, and

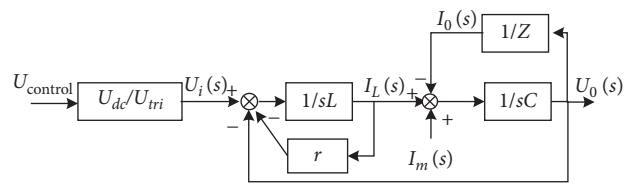

Figure 4: Equivalent dynamic model of the ESS in ESS-integrated PV/wind station.

power line. Define i_{refd} and i_{refq} as the reference of i_d and i_q. Equation (5) is rearranged as

$$\begin{cases} L\dot{e}_{\mathrm{id}} = u_d + \omega L i_q - ri_d - u_{\mathrm{cond}} - L\dot{i}_{\mathrm{refd}}, \\ L\dot{e}_{\mathrm{iq}} = u_q - \omega L i_d - ri_q - u_{\mathrm{conq}} - L\dot{i}_{\mathrm{refq}}, \end{cases} \tag{6}$$

where $e_{\mathrm{id}} = i_d - i_{\mathrm{refd}}$ and $e_{\mathrm{iq}} = i_q - i_{\mathrm{refq}}$. Equation (6) is rearranged as follows:

$$\dot{E} = a\mathbf{I} - b\mathbf{U} + b\mathbf{U}_c + c\mathbf{PI} - \dot{I}_{\mathrm{ref}}, \tag{7}$$

where $\mathbf{E} = [e_{\mathrm{id}} \cdot e_{\mathrm{iq}}]^T$, $\mathbf{I} = [i_{\mathrm{id}} \cdot i_{\mathrm{iq}}]^T$, $\mathbf{U} = [u_{\mathrm{id}} \cdot u_{\mathrm{iq}}]^T$, $\mathbf{U}_c = [u_{\mathrm{cond}} \cdot u_{\mathrm{conq}}]^T$, $\mathbf{I}_{\mathrm{ref}} = [d\mathrm{refd} \cdot q\mathrm{refq}]^T$, and $\mathbf{P} = \begin{bmatrix} 0 & 1 \\ -1 & 0 \end{bmatrix}$. $a = -(r/L), b = -(1/L), c = \omega$.

According to the aforementioned discussion, the ESSs are nonlinear, time-variable system, and there are uncertainties in the ESS-integrated PV/wind station, which are caused by parametric variations or external disturbances. Therefore, equation (7) should be modified as follows:

$$\begin{aligned} \dot{\mathbf{E}} = {} & (a + \Delta a)\mathbf{I} - (b + \Delta b)\mathbf{U} + (b + \Delta b)\mathbf{U}_c + (c + \Delta c)\mathbf{PI} \\ & - \dot{\mathbf{I}}_{\mathrm{ref}} + \mathbf{U}_m, \end{aligned} \tag{8}$$

where $\Delta a, \Delta b$, and Δc represent the system parameter variations and $\mathbf{U}_m$ represents the external disturbances or uncertainties. Define

$$\mathbf{W} = \Delta a\mathbf{I} - \Delta b\mathbf{U} + \Delta b\mathbf{U}_c + \Delta c\mathbf{PI} + \mathbf{U}_m. \tag{9}$$

Thus, equation (8) is rearranged as

$$\dot{\mathbf{E}} = a\mathbf{I} - b\mathbf{U} + b\mathbf{U}_c + c\mathbf{PI} - \dot{\mathbf{I}}_{\mathrm{ref}} + \mathbf{W}. \tag{10}$$

The bound of the uncertainty is assumed to meet the following inequality:

$$|\mathbf{W}| \le \mathbf{Q}, \tag{11}$$

where $\mathbf{Q} = [\mathbf{Q}_d, \mathbf{Q}_q]^T$ represents the unknown positive constants.

4.2. ARSMC System. The proposed control system for ESSs is divided into two main parts, as illustrated in Figure 5. The first part is the primary control which produces the reference signals $\mathbf{I}_{\mathrm{ref}}$ based on $\Delta P_{\Sigma\mathrm{ESSs}}^{\mathrm{request}}$ and the operation mode of ESSs. The second part is the ARSMC system which generates the control signal U_{control}. In this part, the state feedback term gives concise sliding surface while makes full use of

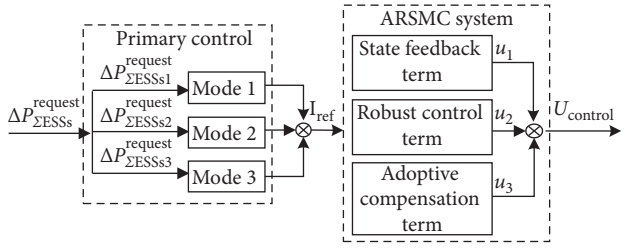

Figure 5: The control system of the ESS in ESS-integrated PV/wind station.

pole assignment and state feedback. Robust control term forms the structure of ESSs model. Adaptive compensation term adjusts the control law based on uncertainties or disturbance in real time. As the disturbance is unknown variables and cannot be specified or determine as a fixed value, introducing an adaptive strategy is a more practical solution.

The control objective of the ARSMC system is to make the output power of the ESSs equal to $\Delta P^{\text{request}}_{\Sigma\text{ESSs}}$. Specifically, it has to enforce i_d, i_q to track its reference i_{refd}, i_{refq} or enforce $\mathbf{I}$ follow its reference $\mathbf{I}_{\text{ref}}$.

First, define a sliding surface as equation (12), to obtain a sliding motion through the entire state trajectory, while eliminate static control error:

$$\mathbf{S} = \mathbf{E} + \int (a - b\mathbf{K})\mathbf{E}ds, \tag{12}$$

where $\mathbf{S} = [\mathbf{S}_d, \mathbf{S}_q]^T$ and $\mathbf{K} = [\mathbf{K}_d, \mathbf{K}_q]^T$ is the control coefficient matrix.

Second, design the control scheme as follows:

$$\mathbf{U}_c = \mathbf{U}_1 + \mathbf{U}_2 + \mathbf{U}_3, \tag{13}$$

where

$$\begin{aligned} \mathbf{U}_1 &= \mathbf{U} + b\mathbf{KI}, \\ \mathbf{U}_2 &= b^{-1}(-\varepsilon \operatorname{sign}(\mathbf{S})) + c\mathbf{PI} + a\mathbf{I} - \dot{\mathbf{I}}_{\text{ref}}, \\ \mathbf{U}_3 &= b\mathbf{S}\operatorname{abs}(-b\mathbf{S})^{-1}\widehat{\mathbf{Q}}, \end{aligned} \tag{14}$$

where $\mathbf{U}_1$ is the state feedback term, $\mathbf{U}_2$ is the robust control term, and $\mathbf{U}_3$ is the adaptive compensation term. ε is a small positive constant, $\operatorname{sign}(\mathbf{S}) = [\operatorname{sign}(s_d) \cdot \operatorname{sign}(s_q)]^T$, being $\operatorname{sign}(\cdot)$ the sign function and $\operatorname{abs}(\cdot)$ the absolute value function. $\widehat{Q}$ is the estimated value of $\mathbf{Q}$; define the parameter deviation as $\widetilde{\mathbf{Q}} = \widehat{\mathbf{Q}} - \mathbf{Q}$ and the adaptive law as

$$\dot{\widehat{\mathbf{Q}}} = \operatorname{abs}(-b\mathbf{S}). \tag{15}$$

Proof. Sliding surface and parameters composing the adaptive law are based on the difference between the nominal nonlinear system and the uncertain nonlinear system, and it satisfies the global Lyapunov stability condition. Using Lyapunov stability analysis to derive the existence condition of the sliding mode and setting the Lyapunov function as

$$\mathbf{V} = \frac{\mathbf{S}^2 + \widetilde{\mathbf{Q}}^2}{2}. \tag{16}$$

Taking the derivative of equation (16),

$$\dot{\mathbf{V}} = \mathbf{S}\dot{S} + \widetilde{\mathbf{Q}}\dot{\widetilde{\mathbf{Q}}}. \tag{17}$$

Taking the derivative of equation (12) along (9) and substituting (13) and (15) into (17) to simplify equation (17) as

$$\dot{\mathbf{V}} = \mathbf{S}\left(-b\mathbf{U}_3 + \varepsilon \operatorname{sign}(\mathbf{S}) + \mathbf{W} + \mathbf{KE}\right) + \widetilde{Q}\dot{\widetilde{\mathbf{Q}}} \le \varepsilon \cdot \operatorname{abs}(\mathbf{S}). \tag{18}$$

Therefore, $\dot{V} < 0$ when $\operatorname{abs}(\mathbf{S}) \neq 0$ which ensures the asymptotically stable behavior for the sliding-mode system on the sliding surface (12).

Once the system trajectory reaches the sliding surface, it yields $\mathbf{S} = \dot{S} = 0$:

$$\dot{S} = a\mathbf{I} - b\mathbf{U} + b\mathbf{U}_c + c\mathbf{PI} - \dot{I}_{\text{ref}} + \mathbf{W} - a\mathbf{E} + b\mathbf{KE} = 0. \tag{19}$$

Deduce the equivalent control from equation (19) as

$$\mathbf{U}_{\text{eq}} = -b^{-1}\left(a\mathbf{I}_{\text{ref}} - b\mathbf{U} + c\mathbf{PI} - \dot{I}_{\text{ref}} + \mathbf{W} - a\mathbf{E} + b\mathbf{KE}\right). \tag{20}$$

Substitute equation (20) into equation (8):

$$\dot{E} = a\mathbf{E} - b\mathbf{KE}. \tag{21}$$

It implies that probably designed state feedback coefficient $\mathbf{K}$ guarantees the robustness of sliding mode (21) along with dynamics features like rising time and maximum overshoot. □

5. Case Studies

A simulation platform under MATLAB environment based on Figure 1 is developed to validate the AGC auxiliary service performance of the ESS-integrated PV/wind station; furthermore, case studies were conducted on the NI-PXI (PCI Extensions for Instrumentation, PXI) platform to verify the proposed ARSMC system as shown in Figure 6.

The key parameters of the developed model are given in Table 1. The ESS-integrated PV/wind station in Figure 1 is connected to the grid through a 380 V/10 kV transformer. A 12 MW synchronous machine in the 10 kV grid works as a conventional regulation power source responds to AGC. According to the sliding surface (12), the control coefficient matrix is designed to guarantee the robustness of the sliding mode show as equation (21), as well as the dynamic performance and stability; set $\mathbf{K} = [0.0180.5]$.

The synchronous machine delivers 10 MW active power to the power grid. The ESSs in ESS-integrated PV/wind station deliver 100 kW active power to the power grid. Set dispatch instruction from AGC $\Delta P^{\text{request}}_{\Sigma}$ to 500 kW to eliminate the frequency deviation. Figure 7 gives the frequency of this 10 kV power system with the synchronous

Figure 6: The NI-PXI platform.

Table 1: Key parameters of ESSs and heat pumps.

ESS parameters	
ESS battery size	50 kWh
DC voltage	1000 V
AC voltage	380 V
Filter capacitance	3 μF
Filter inductance	15 mH
Power system parameters	
Voltage (RMS) (phase)	10 kV
Frequency	50 Hz

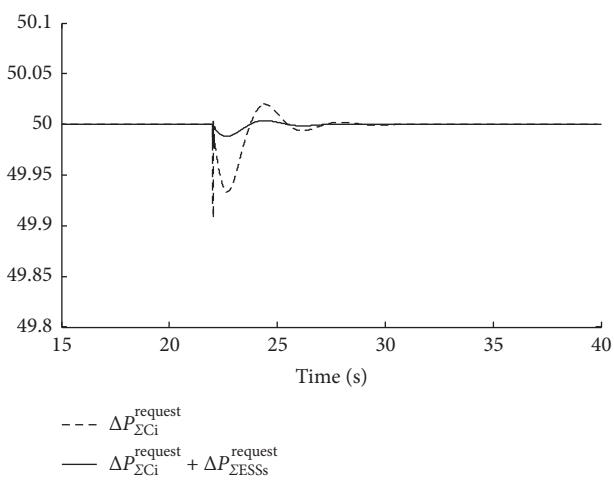

Figure 7: The 10 kV power system frequency.

machine working as a regulation power source response to AGC, which means

$$\Delta P_{\Sigma}^{request} = \sum_{i=1,2,3,\cdots} \Delta P_{\Sigma Ci}^{request} + \sum_{i=1,2,3,\cdots} \Delta P_{\Sigma Li}^{request}, \\ = 500 + 0 = 500\,\text{kW}. \tag{22}$$

Then in the same scenario, both the synchronous machine and ESS-integrated PV/wind station provide AGC auxiliary service, which means

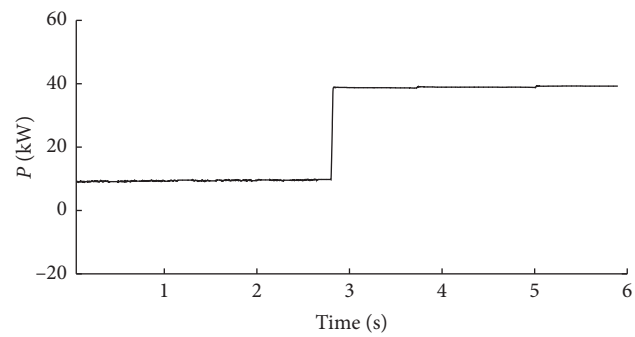

Figure 8: Output power of the ESS (output power increases from 10 kW to 40 kW).

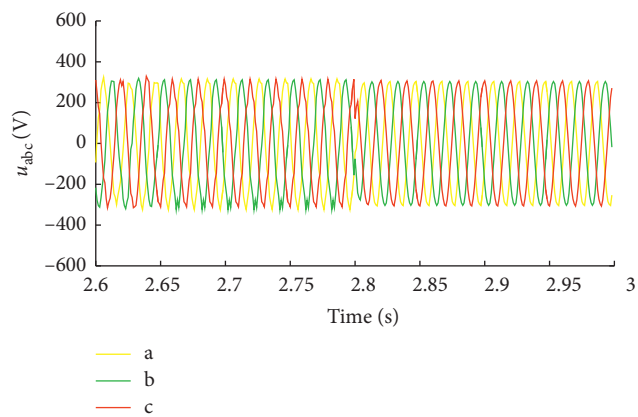

Figure 9: Voltage waveforms of the ESS (output power increases from 10 kW to 40 kW).

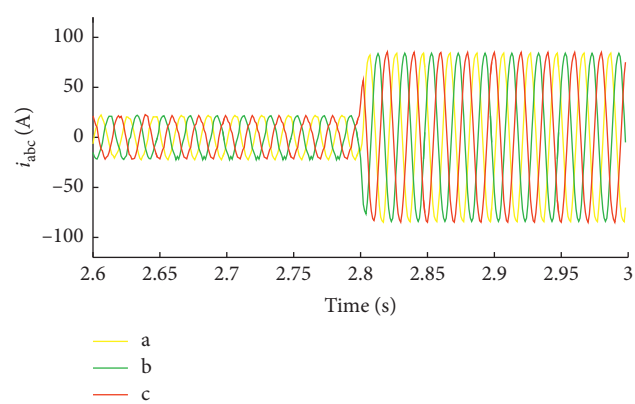

Figure 10: Current waveforms of the ESS (output power increases from 10 kW to 40 kW).

$$\Delta P_{\Sigma}^{request} = \sum_{i=1,2,3,\cdots} \Delta P_{\Sigma Ci}^{request} + \sum_{i=1,2,3,\cdots} \Delta P_{\Sigma Li}^{request}, \\ = 200 + 300 = 500\,\text{kW}, \tag{23}$$

$$\Delta P_{\Sigma L}^{request} = \Delta P_{\Sigma PV}^{request} + \Delta P_{\Sigma wind}^{request} + \Delta P_{\Sigma ESSs}^{request}, \\ = 0 + 0 + 300 = 300\,\text{kW}. \tag{24}$$

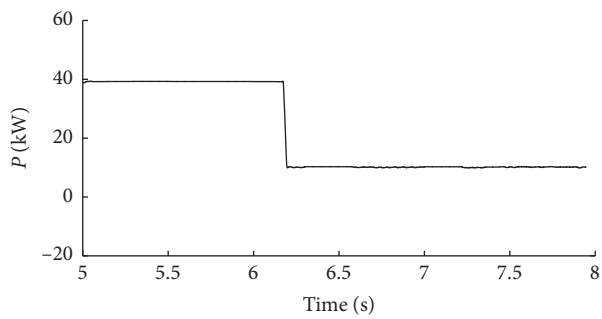

Figure 11: Output power of the ESS (output power falls from 40 kW to 10 kW).

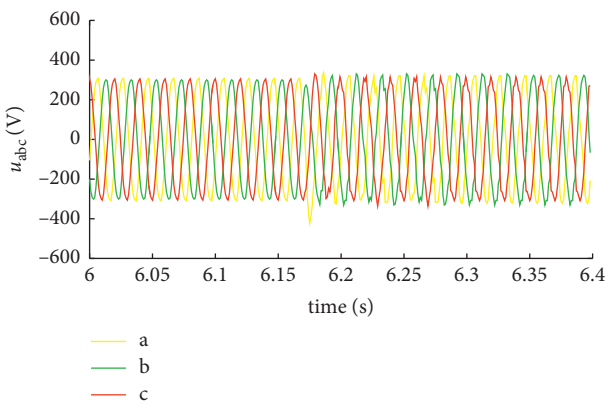

Figure 12: Voltage waveforms of the ESS (output power falls from 40 kW to 10 kW).

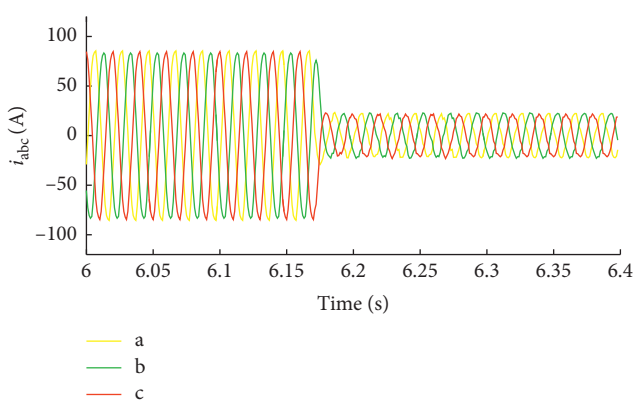

Figure 13: Current waveforms of the ESS (output power falls from 40 kW to 10 kW).

In order to verify an extreme condition, PV and wind generation operate at MPPT mode and only the ESSs respond to AGC. The AGC auxiliary service control can improve the existing AGC control performance with quick response and steady state.

Figure 8 presents output power of one ESS, which is 10 kW at the beginning, and then it goes up to 40 kW response to AGC demand. Voltage and current waveforms at the AC side are shown in Figures 9 and 10. The output

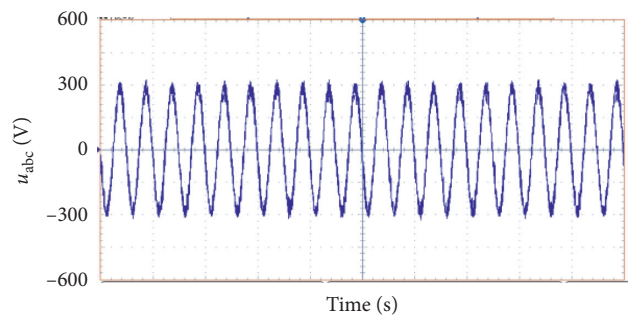

Figure 14: Experimental voltage waveform of the ESS (output power is set to 10 kW).

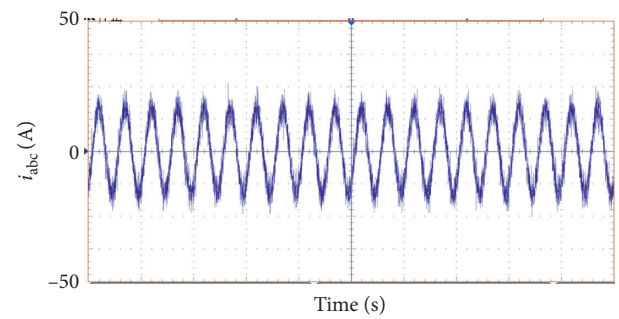

Figure 15: Experimental current waveform of the ESS (output power is set to 10 kW).

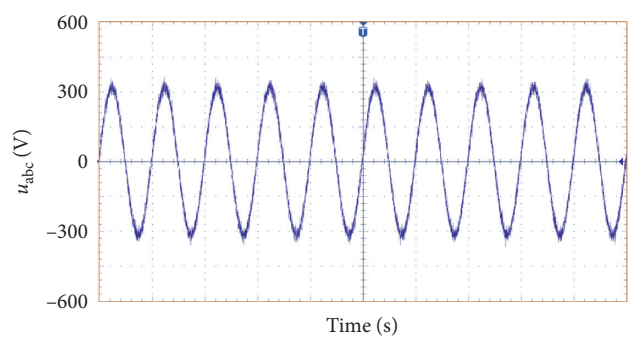

Figure 16: Experimental voltage waveform of the ESS (output power is set to 40 kW).

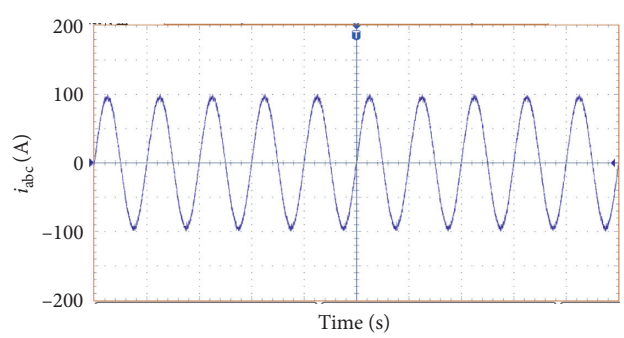

Figure 17: Experimental current waveform of the ESS (output power is set to 40 kW).

current of the ESSs does not have any inrush spikes during the entire transition period, and there is no voltage perturbation along the operation.

Figure 11 presents the output power of one ESS, which is 40 kW at the beginning, and then it falls from 40 kW to 10 kW response to AGC instruction. Its voltage and current waveforms at the AC side are shown in Figures 12 and 13. The output current of the ESSs does not have any inrush spikes during the entire transition period, and there is no voltage perturbation along the operation.

Figures 14 and 15 show the experimental waveforms of the ESS when its output power reference is set at 10 kW. Figure 14 is the voltage waveform of the ESS at the AC side, and Figure 15 is the current waveform of phase A.

Figures 16 and 17 show the experimental waveforms of the ESS when its output power reference is set at 40 kW. Figure 14 is the voltage waveform of the ESS at the AC side, and Figure 15 is the current waveform of phase A.

These results indicate smooth and stable operation of the ESS-integrated PV/wind station and show that the ESSs provide PV and wind generation additional AGC auxiliary service functionality without changing their inner control strategies conceived for MPPT mode.

6. Conclusions

The AGC auxiliary service control proposed in this paper is integrated with existing AGC control strategies. Power grid dispatching center only needs to add instruction allocation module for the ESS-integrated PV/wind stations. It uses ESSs to add regulation capacity and improve dynamic performance of AGC without changing the control strategies of RESs conceived for MPPT mode. As the ESSs are inherently nonlinear and time variable, the mathematical model is built considering the system parameter variations and disturbances or uncertainties. The ARSMC-based ESS control system is proposed to deal these control challenges and improve its stability and dynamic performances. The rigorous proof process verifies the ARSMC strategy mathematically. The case studies on NI-PXI platform shows the fast dynamic response and robustness performance of the ESSs, guaranteeing stable operation of the ESS-integrated PV/wind station, as well as voltage and frequency regulation capability.

The ESSs provide additional AGC auxiliary service functionality without changing RES inner control strategies. The ARSMC-based ESSs is suitable for existing RESs to extend their functions and to form a ESS-integrated PV/wind station. The ESSs are independent from the use of third-party commercial RESs units, which means they do not need specific customized RESs.

Data Availability

The data used to support the findings of the study are included within the article.

Conflicts of Interest

The authors declare that there are no conflicts of interest regarding the publication of this paper.

Acknowledgments

This work is supported by the Research on Key Technologies of Self-Supporting Micro-Renewable Energy Network in Qinghai Agricultural and Pastoral Areas, No. 2018-ZJ-748.

References

[1] W. Liu, G. Geng, Q. Jiang, H. Fan, and J. Yu, "Model-free fast frequency control support with energy storage system," *IEEE Transactions on Power Systems*, vol. 35, no. 4, pp. 3078–3086, 2020.

[2] Y. Wang, Y. Xu, Y. Tang et al., "Aggregated energy storage for power system frequency control: a finite-time consensus approach," *IEEE Transactions on Smart Grid*, vol. 10, no. 4, pp. 3675–3686, 2019.

[3] F. Cheng, L. Qu, W. Qiao, C. Wei, and L. Hao, "Fault diagnosis of wind turbine gearboxes based on DFIG stator current envelope analysis," *IEEE Transactions on Sustainable Energy*, vol. 10, no. 3, pp. 1044–1053, 2019.

[4] V. Knap, S. K. Chaudhary, D.-I. Stroe, M. Swierczynski, B.-I. Craciun, and R. Teodorescu, "Sizing of an energy storage system for grid inertial response and primary frequency reserve," *IEEE Transactions on Power Systems*, vol. 31, no. 5, pp. 3447–3456, 2016.

[5] X. Sun, X. Liu, S. Cheng et al., "Actual measurement and analysis of fast frequency response capability of PV-inverters in northwest power grid," *Power System Technology*, vol. 41, no. 9, pp. 2792–2798, 2017.

[6] Y. Xu, F. Li, Z. Jin, and M. Hassani Variani, "Dynamic gain-tuning control (DGTC) approach for AGC with effects of wind power," *IEEE Transactions on Power Systems*, vol. 31, no. 5, pp. 3339–3348, 2016.

[7] Y. Wei, I. Jayawardene, and G. Kumar Venayagamoorthy, "Optimal automatic generation controllers in a multi-area interconnected power system with utility-scale PV plants," *IET Smart Grid*, vol. 2, no. 4, pp. 581–593, 2019.

[8] C. Wei, Z. Zhang, W. Qiao, and L. Qu, "An adaptive network-based reinforcement learning method for MPPT control of PMSG wind energy conversion systems," *IEEE Transactions on Power Electronics*, vol. 31, no. 11, pp. 7837–7848, 2016.

[9] D. Venkatramanan and V. John, "Dynamic modeling and analysis of buck converter based solar PV charge controller for improved MPPT performance," *IEEE Transactions on Industry Applications*, vol. 55, no. 6, pp. 6234–6246, 2019.

[10] R. B. Bollipo, S. Mikkili, and P. K. Bonthagorla, "Critical review on PV MPPT techniques: classical, intelligent and optimisation," *IET Renewable Power Generation*, vol. 14, no. 9, pp. 1433–1452, 2020.

[11] L. Meng, J. Zafar, S. K. Khadem et al., "Fast frequency response from energy storage systems-a review of grid standards, projects and technical issues," *IEEE Transactions on Smart Grid*, vol. 11, no. 2, pp. 1566–1581, 2020.

[12] X. Xie, Y. Guo, B. Wang, Y. Dong, L. Mou, and F. Xue, "Improving AGC performance of coal-fueled thermal generators using multi-MW scale BESS: a practical application," *IEEE Transactions on Smart Grid*, vol. 9, no. 3, pp. 1769–1777, 2018.

[13] W. Tasnin and L. C. Saikia, "Performance comparison of several energy storage devices in deregulated AGC of a multi-area system incorporating geothermal power plant," *IET Renewable Power Generation*, vol. 12, no. 7, pp. 761–772, 2018.

[14] B. Mantar Gundogdu, D. T. Gladwin, S. Nejad, and D. A. Stone, "Scheduling of grid-tied battery energy storage

system participating in frequency response services and energy arbitrage," *IET Generation, Transmission & Distribution*, vol. 13, no. 14, pp. 2930–2941, 2019.

[15] Y. Cheng, M. Tabrizi, M. Sahni, A. Povedano, and D. Nichols, "Dynamic available AGC based approach for enhancing utility scale energy storage performance," *IEEE Transactions on Smart Grid*, vol. 5, no. 2, pp. 1070–1078, 2014.

[16] K. Doenges, I. Egido, L. Sigrist, E. Lobato Miguélez, and L. Rouco, "Improving AGC performance in power systems with regulation response accuracy margins using battery energy storage system (BESS)," *IEEE Transactions on Power Systems*, vol. 35, no. 4, pp. 2816–2825, 2020.

[17] F. Zhang, Z. Hu, K. Meng, L. Ding, and Z. Dong, "HESS sizing methodology for an existing thermal generator for the promotion of AGC response ability," *IEEE Transactions on Sustainable Energy*, vol. 11, no. 2, pp. 608–617, 2020.

[18] Y. Wang, C. Wan, Z. Zhou, K. Zhang, and A. Botterud, "Improving deployment availability of energy storage with data-driven AGC signal models," *IEEE Transactions on Power Systems*, vol. 33, no. 4, pp. 4207–4217, 2018.

[19] P. Thounthong, A. Luksanasakul, P. Koseeyaporn, and B. Davat, "Intelligent model-based control of a standalone photovoltaic/fuel cell power plant with supercapacitor energy storage," *IEEE Transactions on Sustainable Energy*, vol. 4, no. 1, pp. 240–249, 2013.

[20] M. Datta and T. Senjyu, "Fuzzy control of distributed PV inverters/energy storage systems/electric vehicles for frequency regulation in a large power system," *IEEE Transactions on Smart Grid*, vol. 4, no. 1, pp. 479–488, 2013.

[21] A. Moeini, I. Kamwa, Z. Gallehdari, and A. Ghazanfari, "Optimal robust primary frequency response control for battery energy storage systems," in *Proceedings of the 2019 IEEE Power & Energy Society General Meeting (PESGM)*, pp. 1–5, Atlanta, GA. USA, August 2019.

[22] S. Zhang, Y. Mishra, and M. Shahidehpour, "Fuzzy-logic based frequency controller for wind farms augmented with energy storage systems," *IEEE Transactions on Power Systems*, vol. 31, no. 2, pp. 1595–1603, 2016.

[23] C. Wei, M. Benosman, and T. Kim, "Online parameter identification for state of power prediction of lithium-ion batteries in electric vehicles using extremum seeking," *International Journal of Control, Automation and Systems*, vol. 17, no. 11, pp. 2906–2916, 2019.

[24] Q. Chen, H. Shi, and M. Sun, "Echo state network-based backstepping adaptive iterative learning control for strict-feedback systems: an error-tracking approach," *IEEE Transactions on Cybernetics*, vol. 50, no. 7, pp. 3009–3022, 2020.

[25] Q. Chen, H. Shi, and M. Sun, "Echo state network based backstepping adaptive iterative learning control for strict-feedback systems: an error-tracking approach," *IEEE Transactions on Cybernetics*, vol. 50, no. 7, pp. 3009–3022, 2019.

[26] Q. Chen, S. Xie, M. Sun, and X. He, "Adaptive nonsingular fixed-time attitude stabilization of uncertain spacecraft," *IEEE Transactions on Aerospace and Electronic Systems*, vol. 54, no. 6, pp. 2937–2950, 2018.

[27] Q. Chen, X. Yu, M. Sun, C. Wu, and Z. Fu, "Adaptive repetitive learning control of PMSM servo systems with bounded nonparametric uncertainties: theory and experiments," *IEEE Transactions on Industrial Electronics*, 2020.

[28] J. Na, Y. Li, Y. Huang, G. Gao, and Q. Chen, "Output feedback control of uncertain hydraulic servo systems," *IEEE Transactions on Industrial Electronics*, vol. 67, no. 1, pp. 490–500, 2020.

[29] V. Utkin, "Variable Structure system with sliding modes," *IEEE Transactions on Automatic and Control*, vol. 22, no. 2, pp. 212–222, 1979.

[30] V. Utkin, I. Guldner, and J. X. Shi, *Sliding Mode Control in Electromechanical System*, Taylor and Francis, London, UK, 1999.

[31] S. Wang, L. Tao, Q. Chen, J. Na, and X. Ren, "USDE-based sliding mode control for servo mechanisms with unknown system dynamics," *IEEE/ASME Transactions on Mechatronics*, vol. 25, no. 2, pp. 1056–1066, 2020.

[32] D. Xu, Q. Liu, W. Yan, and W. Yang, "Adaptive terminal sliding mode control for hybrid energy storage systems of fuel cell, battery and supercapacitor," *IEEE Access*, vol. 7, pp. 29295–29303, 2019.

[33] R. Zhang and B. Hredzak, "Nonlinear sliding mode and distributed control of battery energy storage and photovoltaic systems in AC microgrids with communication delays," *IEEE Transactions on Industrial Informatics*, vol. 15, no. 9, pp. 5149–5160, 2019.

[34] V. Patel, D. Guha, and S. Purwar, "Frequency regulation of an islanded microgrid using integral sliding mode control," in *Proceedings of the 2019 8th International Conference on Power Systems (ICPS)*, pp. 1–6, Jaipur, India, December 2019.

[35] Y. Mi, X. He, X. Hao et al., "Frequency control strategy of multi-area hybrid power system based on frequency division and sliding mode algorithm," *IET Generation, Transmission & Distribution*, vol. 13, no. 7, pp. 1145–1152, 2019.

[36] Z. Afshar, N. T. Bazargani, and S. M. T. Bathaee, "Virtual synchronous generator for frequency response improving and power damping in microgrids using adaptive sliding mode control," in *Proceedings of the 2018 International Conference and Exposition on Electrical and Power Engineering (EPE)*, pp. 199–204, Iasi, Romania, October 2018.

[37] C. Swetha, N. S. Jayalakshmi, K. M. Bhargavi, and P. B. Nempu, "Control strategies for power management of PV/battery system with electric vehicle," in *Proceedings of the 2019 IEEE International Conference on Distributed Computing, VLSI, Electrical Circuits and Robotics (DISCOVER)*, pp. 1–6, Manipal, India, August 2019.

[38] I. Kim, "A technique for estimating the state of health of lithium batteries through a dual-sliding-mode observer," *IEEE Transactions on Power Electronics*, vol. 25, no. 4, pp. 1013–1022, 2010.

[39] H. Delavari and S. Naderian, "Backstepping fractional sliding mode voltage control of an islanded microgrid," *IET Generation, Transmission & Distribution*, vol. 13, no. 12, pp. 2464–2473, 2019.

[40] T. Morstyn, A. V. Savkin, B. Hredzak, and V. G. Agelidis, "Multi-agent sliding mode control for state of charge balancing between battery energy storage systems distributed in a DC microgrid," *IEEE Transactions on Smart Grid*, vol. 9, no. 5, pp. 4735–4743, 2018.

[41] M. B. Delghavi, S. Shoja-Majidabad, and A. Yazdani, "Fractional-order sliding-mode control of islanded distributed energy resource systems," *IEEE Transactions on Sustainable Energy*, vol. 7, no. 4, pp. 1482–1491, 2016.

[42] M. I. Ghiasi, M. A. Golkar, and A. Hajizadeh, "Lyapunov based-distributed fuzzy-sliding mode control for building integrated-DC microgrid with plug-in electric vehicle," *IEEE Access*, vol. 5, pp. 7746–7752, 2017.

[43] F. Sebaaly, H. Vahedi, H. Y. Kanaan, N. Moubayed, and K. Al-Haddad, "Sliding mode fixed frequency current controller design for grid-connected NPC inverter," *IEEE Journal of*

Emerging and Selected Topics in Power Electronics, vol. 4, no. 4, pp. 1397–1405, 2016.

[44] B. Wang, J. Xu, R.-J. Wai, and B. Cao, "Adaptive sliding-mode with hysteresis control strategy for simple multimode hybrid energy storage system in electric vehicles," *IEEE Transactions on Industrial Electronics*, vol. 64, no. 2, pp. 1404–1414, 2017.

[45] X. Su, M. Han, J. Guerrero, and H. Sun, "Microgrid stability controller based on adaptive robust total SMC," *Energies*, vol. 8, no. 3, pp. 1784–1801, 2015.